Applied Catalysis B: Environmental 205 (2017) 605–614

Contents lists available at ScienceDirect

Applied Catalysis B: Environmental

journal homepage: www.elsevier.com/locate/apcatb

DFT study of Ni-catalyzed plasma dry reforming of methane

Mahdi Shirazi*, Erik C. Neyts, Annemie Bogaerts

Research Group PLASMANT, Department of Chemistry, University of Antwerp, Belgium

ARTICLE INFO

Article history:
Received 15 October 2016
Received in revised form
23 December 2016
Accepted 3 January 2017
Available online 4 January 2017

Keywords:
DFT
Plasma catalysis
Reaction kinetics
Reaction energetics

ABSTRACT

We investigated the plasma-assisted catalytic reactions for the production of value-added chemicals from Ni-catalyzed plasma dry reforming of methane by means of density functional theory (DFT). We inspected many activation barriers, from the early stage of adsorption of the major chemical fragments derived from CH_4 and CO_2 molecules up to the formation of value-added chemicals at the surface, focusing on the formation of methanol, as well as the hydrogenation of C_1 and C_2 hydrocarbon fragments. The activation barrier calculations show that the presence of surface-bound H atoms and in some cases also remaining chemical fragments at the surface facilitates the formation of products. This implies that the hydrogenation of a chemical fragment on the hydrogenated crystalline surface is energetically favoured compared to the simple hydrogenation of the chemical fragment at the bare Ni(111) surface. Indeed, the presence of hydrogen modifies the electronic structure of the surface and the course of the reactions. We therefore conclude that surface-bound H atoms, and to some extent also the remaining chemical fragments at the crystalline surface, induce the following effects: they facilitate associative desorption of methanol and ethane by increasing the rate of H-transfer to the adsorbed fragments while they impede hydrogenation of ethylene to ethane, thus promoting again the desorption of ethylene. Overall, they thus facilitate the catalytic conversion of the formed fragments from CH_4 and CO_2, into value-added chemicals. Finally, we believe that the retention of methane fragments, especially CH_3, in the presence of surface-bound H atoms (as observed here for Ni) can be regarded as an identifier for the proper choice of a catalyst for the production of value-added chemicals.

1. Introduction

Global warming is a consequence of the rise in the concentration of greenhouse gases in the earth's atmosphere. This rise started since the beginning of the industrial revolution, and resulted in an increase in the global air and sea surface temperature [1]. The two most abundant greenhouse gases are carbon dioxide (CO_2) and methane (CH_4). The atmospheric concentration of CO_2 continues to increase by burning fossil fuels and clearing of native forests. Also the methane concentration has been rising as a consequence of human activities such as leakage from natural gas systems and the raising of livestock.

Dry reforming of methane (DRM) is a method to convert both greenhouses gases into syngas [2]. This is desirable for many industrial synthesis processes [3]. DRM proceeds according to the following reaction:

$$CO_2 + CH_4 \Leftrightarrow 2H_2 + 2CO \qquad \Delta H^{\circ}_{298^{\circ}} = 247\,kJ/mol$$

Both CO_2 and CH_4 molecules are chemically inert and thermodynamically stable. In conventional methods, the conversion of these gases into syngas (or other value-added chemicals) occurs in the presence of a metal-based catalyst at high temperature and pressure (catalyst-based dry reforming) [2,4]. Alternatively, it can also take place in a plasma at room temperature and atmospheric pressure (plasma-based dry reforming) [5]. Both methods face difficulties. Catalyst-based dry reforming is sensitive to coke deposition [6] and subject to a slow start-up time. Plasma-based dry reforming shows a lack of selectivity [7–10].

However, it has been shown that combining the catalyst with a plasma may result in a synergy between both [9,11]. Such synergic interaction between reactive species in the plasma and the catalyst surface may yield a more favorable process, in terms of e.g. improved selectivity and energy efficiency. The combination of plasma and catalyst may also initiate chemical reactions at lower temperatures than in the conventional thermo-chemical process [12,13].

Non-thermal plasmas are highly reactive, due to the presence of energetic electrons and reactive species (free radicals, excited molecules, and ions) [9,14,15]. The energetic electrons, with a typical energy of 1–10 eV, create a distinct non-equilibrium plasma

* Corresponding author.
E-mail address: mahdi.shirazi@uantwerpen.be (M. Shirazi).

http://dx.doi.org/10.1016/j.apcatb.2017.01.004
0926-3373/

with an overall gas kinetic temperature as low as room temperature.

Hence, plasma catalysis performs at much lower pressure and temperature than thermal catalysis. However, the net effect is the formation of abundant surface-bound H atoms at the surface. This ultimately gives rise to the facilitation of hydrogenation reactions in both processes (i.e., thermal and plasma catalysis), no matter which reaction condition is considered. In this sense, there is no major difference in the model construction and computational details between thermal and plasma catalysis. A difference in reaction chemistry, however, may arise from the different number of surface-bound H atoms.

H-adsorption or H_2 dissociation on a Ni(111) surface is an exothermic reaction up to a certain H-coverage which depends on the reaction condition. The H-coverage, therefore, modifies the initial energy of the system. Here, for each chemical reaction the initial structure/state is considered as the reference state which makes the comparison of barriers easier.

To model the atomistic behavior of this system [16,17], the interaction of all plasma species with the catalyst surface should be considered, in principle taking the nanoscale features of the catalyst into account as well [18,19]. This entails simulating the interaction of all reactive species with the various possible surface configurations, such as terraces, steps, kinks, and clusters. Moreover, the catalyst surface is also subject to modification under the influence of the plasma [20,21]. Once the overall interactions and surface modifications are identified, the gathered information from the atomistic model can be used as raw data for the development of classical force fields for plasma catalysis [22,23], for a coarse-grained model [24] or as input for a plasma chemistry model [25–27]. The ultimate goal of this research is to implement the gathered information into a kinetic Monte-Carlo model (KMC) to investigate the dominant products in different reaction conditions.

To investigate the formation of value-added chemicals in plasma catalysis, we performed detailed DFT calculations as reported in the present paper. The main objective is to explain the reaction kinetics at low temperature, characteristic for a non-thermal plasma. In this sense, the effect of surface-bound H atoms and remaining chemical fragments at the surface on the chemical reactions is considered. This is consistent with earlier work [28], where it was observed that the remaining chemical fragments activate the chemical reactions. Those neighbors do not participate directly (stoichiometrically or catalytically) in the chemical reaction. However, they do modify the potential energy surface of the system.

In many studies [29,30], the influence of remaining chemical fragments on the reaction energetics and reaction kinetics of a desired reaction is ignored for the sake of simplicity. In this contribution, we will show how remaining chemical species, especially surface-bound H atoms, modify the potential energy surface (PES) to facilitate a chemical reaction.

In this paper, we show that the surface-bound H atoms play a vital role in facilitating the hydrogenation of oxygen compounds and hydrocarbons into the major products of plasma catalysis [8,12]. Since the reaction kinetics is inspected for a relatively large H-coverage, the surface-bound species first should be involved in direct interaction with surface-bound H atoms rather than with the other surface-bound species (adsorbate–adsorbate interaction) [31]. Hence, the lifetime of the surface-bound species is short and they would desorb before interacting with the other surface-bound species.

The increase of H-coverage gives rise to weaker adsorption of the "organic" fragments. A relationship between the thermodynamics and the activation barrier often found to hold is the so-called Bronsted-Evans-Polanyi (BEP) relation [32], which states that in a family of reactions, the change in reaction energy scales linearly with the change in reaction barrier. As we will show below, however, we observe that while there is indeed a relationship between the change in activation barrier and change in reaction energy as a function of H-coverage, the scaling is not linear.

As mentioned above, plasma catalysis may perform better at low temperatures than thermal catalysis. The reported activation barriers [33,34] for dissociative adsorption of neutral molecules in DRM are relatively large. For instance, the activation energy for dissociative chemisorption of methane on the crystalline Ni(111) surface was reported to be 1.17 eV. The reported activation energy for dissociative adsorption of excited methane is slightly smaller, 0.95 eV [35]. Hence, these chemical reactions are less likely to be kinetically active at the low temperatures characteristic for plasma catalysis, which is in contrast to the better performance observed for plasma catalysis at low temperatures.

The interaction of electronically excited molecules with the surface cannot be studied by conventional ground state DFT calculations. This type of interaction can be studied by time-dependent DFT. However, here we assumed that upon dissociation of molecules in the plasma phase, they are mostly formed in their electronic ground state, and upon interaction with the surface also adsorb in their electronic ground state. This assumption corresponds to both experimental and modeling results, indicating that the densities/fluxes of electronically excited species are typically many orders of magnitude lower than the density of ground state species. Based on this assumption, we consider the possible formation of products starting from the main fragments. We acknowledge that in certain types of plasma, e.g. in microwave discharges, vibrationally excited states might be of importance [36–38]. However, plasma dry reforming is mostly performed in dielectric barrier type discharges, in which the vibrationally excited states are not highly populated [36–38]. The above references apply to CO_2, but vibrational excitation of CH_4 is stated to be anyway of lower importance than vibrational excitation of CO_2, in a CO_2/CH_4 mixture [36].

Here, we therefore assume that radical fragments derived from CH_4 and CO_2 molecules are already chemically adsorbed. These adsorbed species may be incoming free radicals produced in the plasma [9], or they can be products of chemical reactions. The adsorption enthalpies for radical fragments derived from CH_4 and CO_2 on Ni were extensively studied before [33,39]. Here, we thus mainly focus on the reaction kinetics of the associative desorption of products of these fragments in plasma catalysis.

We mainly focus on the production of methanol and C_2 hydrocarbons that were measured experimentally as two main added value products in plasma catalysis of CO_2 and CH_4. In most cases, the experiments are carried out under atmospheric pressure and a moderate temperature and the plasma zone is kept at room temperature. The dielectric barrier discharge reactor is mainly used by an AC high voltage power supply with a variable voltage of 1–25 kV and a variable frequency of 20–60 kHz [8,12,40].

In plasma catalysis, the formation of products occurs through the Eley-Rideal (ER) and the Langmuir-Hinshelwood (LH) mechanism. This is different from thermal catalysis, where most catalytic reactions proceed via the LH mechanism [41]. In plasma catalysis, not all impacts of free radicals necessarily lead to the formation of a product. If an impingement gives rise to the formation of a closed shell molecule, it mainly terminates to the associative desorption of the closed shell molecule. In the context of atomic orbitals, a closed shell configuration is a valence shell which is completely filled with electrons. In contrast, an open shell configuration is not completely filled with electrons. For instance, the interaction between an incoming CH_3 radical from the plasma and an adsorbed H atom gives rise to the associative desorption of CH_4 (ER mechanism). In contrast, if an impingement gives rise to the formation of an open shell molecule, the formed molecule remains as an adsorbate. For instance, the interaction between an incoming CH_3 radical

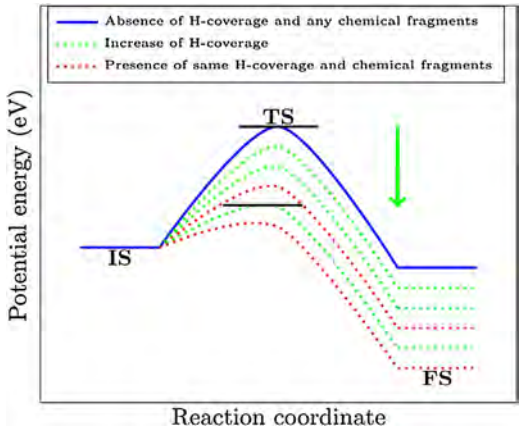

Scheme 1. Schematics of a typical energy diagram for hydrogenation of chemical fragments on Ni(111), starting from the initial state (IS), over the transition state (TS), and ending in the final state (FS), for different H-coverage and the absence or presence of other chemical fragments. The presence of surface-bound H atoms gives rise to a reduction in both the activation energy and the reaction energy (green arrow), while the presence of other chemical fragments can result in either a rise or a reduction of the activation energy and reaction energy. (For interpretation of the references to colour in this figure legend, the reader is referred to the web version of this article.)

from the plasma and an adsorbed O atom gives rise to the formation of an adsorbed OCH_3 molecule.

2. Computational details

To study the interaction of free radicals with a Ni catalyst, self-consistent DFT calculations in the GGA approximation are employed. Reaction energies, activation energies and ab initio molecular dynamics (AIMD) of the system are calculated in a 3D periodic model, utilizing VASP [42]. In these calculations, the electronic energies are approximated using the projector augmented wave (PAW) [43] description of atomic cores and the functional of Perdew, Burke, and Ernzerhof (PBE) [44]. The plane wave cut-off energy is set to 400 eV (see Supporting information, Fig. S1). For Ni atoms $3d^8 4s^2$, O atoms $2s^2 2p^4$, and C atoms $2s^2 2p^2$, electrons are included as valence electrons. The self-consistent steps are converged to an energy difference of at least 10^{-4} eV.

Geometries are optimized using the conjugate-gradient scheme without symmetry restraints or fixed atoms, to a convergence of energy gradients of less than 10^{-3} eV/Å. Since the magnetic properties of nickel are essential for an accurate description of the energetics and kinetics [45], all calculations are spin-polarized.

Converged values of the surface energies of the (111) surfaces showed that five layers of Ni are enough to be considered as a slab. The structure of the assumed Ni(111) is explained in previous studies [39]. To avoid slab–slab interaction in the periodic model, a vacuum region of 10 Å above the surface is imposed. The k-point sampling in reciprocal space is generated by the Monkhorst-Pack method. $8 \times 8 \times 8$ and $4 \times 4 \times 1$ grid sizes are utilized for bulk and slab, respectively. For the surface, we use a five-layered 4×4 supercell and the k-point sampling is reduced to $2 \times 2 \times 1$. Hence, each layer of the slab has sixteen Ni atoms.

The AIMD calculations are performed within the micro-canonical ensemble [46]. The Verlet algorithm is used to integrate Newton's classical equations of motion for the ions. A time step of 1 fs is found to be sufficiently small for all frequencies of oscillation in the system. The calculations are done for 400 ionic steps. The initial temperature for assigning random velocities is varied from 300 to 500 K, according to experiments [12,13].

In this study, we extensively use the nudged elastic band (NEB) method [47], to calculate the activation energy for reactions under different local chemistries [48]. Furthermore, AIMD simulations are performed to gain insight in the dynamics of the reaction, which may in some cases deviate from the reaction path predicted by NEB. For instance, if the surface is covered with a large number of H atoms, the selection of the transferred H to a chemical fragment in NEB is based on the shortest distance between the H atom and the chemical fragment, which is not necessarily true.

However, one is confronted with the obstacle of rare events in AIMD simulations. This means that the system is trapped in some local minimum for a long period of time (relative to the AIMD time-scale) and cannot cross the activation barrier to a new minimum. To observe the crossing of a barrier, either alternative simulation techniques such as the recently developed collective-variable driven hyperdynamics method (CVHD) [49] or very long time-scale simulations would be needed. In a AIMD context, however, both would require very long calculation times.

Since the energy minimum of the system is constantly modified by adding new atoms to the surface, the underlying reaction kinetics and reaction energetics of all occurring chemical processes are constantly modified as well. Indeed, the increase or decrease of the coverage of a chemical species generally modifies the rates of the occurring chemical reactions, due to an increase or decrease of the activation energy, and thus it either inhibits or facilitates these reactions. We therefore calculated the plausible crossing of barriers by the NEB method and checked the activation barriers of a chemical reaction in different local chemistries.

Adsorption of H atoms can occur either through impingement from the plasma or as a product of chemical surface reactions. In both cases, H atoms are transferred into a fcc or hcp site at the crystalline surface. H diffusion is a crucial feature and is ultimately required for the formation of the desired products. The presence of H atoms at the surface essentially influences the reaction kinetics of the chemical reactions. As mentioned above, this may either inhibit or facilitate a chemical reaction through the rise or reduction of the activation barrier.

Occasionally, in the case when the activation energy increases, a competitive chemical reaction dominates the chemical process and hinders the chemical reaction of interest. On the other hand, when the activation energy is decreased sufficiently, it will not remain a rare event, since the chemical reaction now occurs much faster (relative to the rare events). This means that the chemical reaction of interest can be observed in the short time-scale accessible to the AIMD simulation. Both cases are observed during optimization or during the AIMD calculations and are included in the supporting information (SI). This will help to establish the trend of a chemical reaction in different local chemistries.

The energy barrier of associative desorption of H_2 from the Ni(111) surface does not reduce to below 0.7 eV within the H-coverage of 0.25–1.0 ML. Hence, the rate of H_2 desorption does not change with the concentration of adsorbed H-atoms up to a H-coverage of 1.0 ML. Desorption of H_2 is indeed a competitive reaction that we are currently investigating. As mentioned above, these competitive reactions with hydrogenation of chemical fragments should be implemented into KMC to address the experimental data more accurately.

The energy difference between two optimized minima gives the reaction energy. Often, in a reaction, two molecules are formed of which one desorbs from the surface while the other remains adsorbed. This gives rise to the relocation of pre-existing atoms at the surface (e.g., H atoms). The activation barrier is calculated as the maximum energy along the reaction coordinate connecting the two minima.

Once the required minimum energy to cross the barrier is detected on the association or dissociation channel, this value is reported as the activation barrier. Occasionally, no activation barrier is detected. In this case, we report the activation barrier as zero

for an exothermic reaction, and as the reaction energy (ΔE) for an endothermic reaction. In all calculations, all other degrees of freedom are optimized. The number of images is modified from 10 to 18 for those reaction paths, depending on the distance that atoms should travel, including end images.

In several cases, the obtained reaction barriers were larger than 1 eV. This is too high for typical process temperatures of plasma catalysis (i.e., below 500 K). Hence, these reactions are not reported here. Indeed, they will not be important for plasma catalysis, where many other reactions, involving radicals, will occur more easily.

The vibrational frequencies of the systems are calculated within the harmonic approximation. The matrix of the second derivatives of the energy with respect to the atomic positions (Hessian matrix) is calculated numerically by displacing each atom twice (±0.015 Å) independently from its equilibrium position in the direction of each Cartesian coordinate. The adsorbate atoms in a chemical reaction and their first metal neighbour atoms are included in the frequency calculation, and thus adsorbate-metal coupling was considered in this calculation.

3. Results and discussions

3.1. Formation and desorption of methanol

In this section, we study the possible reaction pathways for the formation of methanol at the crystalline Ni(111) surface, which is an interesting value-added product [12]. This is initially studied by the introduction of a CH_3 radical to a surface-adsorbed CO_2 molecule (Fig. S2a). This will not give rise to the dissociation of the C—O bond. Indeed, an activation energy of 1.54 eV for desorption of CH_3O is calculated. Similarly, a CH_3 radical is introduced to an adsorbed CO molecule (Fig. S2b). The calculated activation energy of desorption of CH_3O in this case is also very large (3.09 eV). Furthermore, the CO_2CH_3 molecule can also be formed in the plasma and directly adsorb at the Ni(111) surface. However, in all the cases investigated, dissociation of an adsorbed CO_2CH_3 molecule did not occur.

However, the introduction of a H atom to surface-adsorbed CO_2CH_3 can cause the formation of methanol and a CO molecule. This occurs either through H atoms from the plasma or by the transfer of a surface-adsorbed H atom, corresponding to the ER and LH mechanisms, respectively.

The introduction of a H atom from the plasma to an adsorbed CO_2CH_3 fragment through the O atom which is not bound to the surface causes the formation of methanol (CH_3OH) and a surface-adsorbed CO molecule (Fig. S3). This reaction is exothermic by 3.07 eV. However, if the impinging H atom interacts with the CH_3 group instead of with the O atom, methane is formed rather than methanol. Hence, this reaction pathway is not selectively controlled by the catalyst.

Surface transfer of H to the adsorbed CO_2CH_3 fragment also leads to associative desorption of methanol, as shown in Fig. 1a (top view). In this reaction pathway, transfer from the hcp site (pink atom) breaks the bond between C—O (Fig. 1b). This causes the formation of methanol and a CO molecule. Methanol desorbs from the surface while CO is tightly bound to the surface. As a result, the pre-adsorbed atomic H atoms are relocated (green atoms). The relocation of H atoms is correlated to the associative desorption of methanol and binding of the CO molecule, which is all considered in the dissociation channel. In the transition state (Fig. 1b), all H atoms involved in the reaction pathway are located at bridge sites. The H atoms are relocated from the fcc to the hcp sites.

The activation energy of H-transfer is calculated for different H-coverages, as reported in Table 1 (reactions 1–3). The same H atom is considered for each coverage. The activation energy is 0.94 eV at a coverage of 0.50 ML of H, and increases to 1.47 eV at 0.75 ML of H coverage, after which it decreases to 0.66 eV at 1 ML of H coverage. Thus, the activation energy is further reduced upon higher H-coverage. Likewise, the released chemical energy due to the formation of methanol and the binding of CO molecules is increased from 0.86 eV at 0.50 ML of H coverage to 1.26 eV at 0.75 ML of H coverage, but it decreases to 0.75 eV at 1 ML of H coverage. The high coverage of H atoms (1 ML of H) seems to prevent CO molecules binding tight to the surface. Hence, the released chemical energy decreases upon increasing H-coverage. This reaction pathway should anyway be thermally activated by the proper formation of a CO_2CH_3 fragment and a high concentration of H atoms at the crystalline surface. This also implies that the formed open shell molecule (e.g. CO_2CH_3) in the plasma can easily adsorb at the surface and then dissociate to the favoured products in the presence of surface-bound H atoms.

Another possible reaction pathway for methanol formation is the interaction between a surface-adsorbed COH fragment and a CH_3 radical from the plasma. The adsorbed COH can be created by bonding of H atoms from the plasma to an adsorbed CO molecule. Upon impingement of a CH_3 radical from the plasma to the COH fragment at the surface, two different products may be formed, depending on the direction of the incoming CH_3 radical. When the CH_3 radical interacts with the H atom, methane is formed (Fig. S5). If in contrast the CH_3 radical reacts with the O atom, methanol is formed (Fig. S6). Both reactions are exothermic, by 2.84 eV and 0.29 eV, respectively, following the ER mechanism. Thus, this reaction pathway to the formation of methanol cannot be selectively controlled by the catalyst, as it depends again on the direction of the incoming CH3 radical.

So far, the identified reaction pathways leading to the formation of methanol were not selective or showed a relatively large activation energy. In the following discussion, those reactions that can selectively cause methanol formation with low activation energies are considered.

The interaction of an O atom from the plasma with an adsorbed fragment of methane leads to the formation of an oxygenated fragment (Fig. S7). The retention of the methane fragment by the catalyst and a proper flux of O atoms are the key factors for the formation of methanol through this reaction pathway. Since hydrogenation of C and CH fragments readily occurs at high H coverage (see Section 3.2 below), O atoms less likely react with C and CH fragments at the surface, and thus, the interaction of O atoms with C and CH fragments is ignored in the following. We only consider the interaction of O atom with CH_2 and CH_3 fragments, as well as the subsequent hydrogenation of the oxygenated fragments to form methanol.

The introduction of O atoms to the CH_3 group causes the formation of CH_2OH (Fig. S7a and b). This adsorbed molecule is chemically bound to the top of a Ni atom at the surface. This reaction is a preliminary step to the formation of methanol, and is strongly exothermic by 4.93 eV (Table 1, reaction 4).

The subsequent hydrogenation of CH_2OH to methanol is considered for different H-coverages, as well as the presence of other chemical fragments, as reported in Table 1 (reactions 5–10). As depicted in Fig. 5, the increase of H-coverage from 0.25 to 0.75 ML causes a reduction in activation energy for hydrogenation from 0.59 eV to 0.14 eV (Table 1, reactions 5–7). Furthermore, the introduction of chemical fragments at neighboring sites also shows a reduction in activation energy (Table 1, reactions 8–10).

The side and top view of the reaction pathway is shown in the insets in Fig. 2. H-transfer from the hcp site (pink atom) to the oxygenated species at the top of the Ni site leads to the associative desorption of methanol from the surface. This associative desorption occurs at a coverage of 0.75 ML of H. A H atom at the fcc site (green atom) is transferred to the previously occupied hcp site. The relocation of H atoms at the surface can be seen in the top view

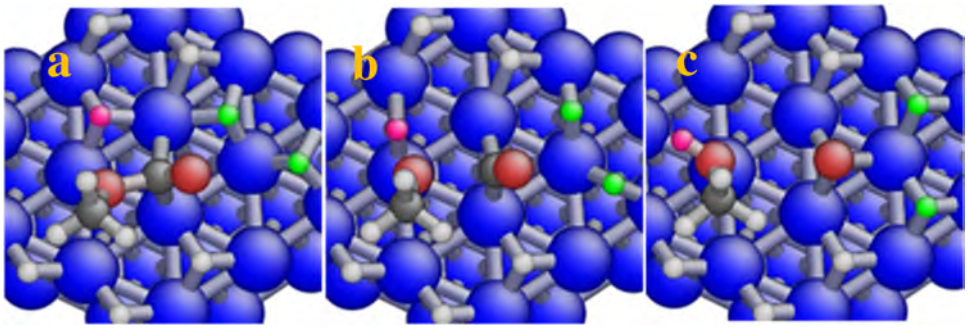

Fig. 1. Top view of H-transfer from the surface to adsorbed CO_2CH_3. H-transfer is indicated by the pink atom. (a) Initial configuration of the adsorbed CO_2CH_3 fragment at a coverage of 0.50 ML of H. (b) Transition state. H-transfer to O breaks the bond between C and O. All H atoms are located at the bridging site. (c) Associative desorption of methanol and an adsorbed CO molecule (See Fig. S4). Transfer of a CO molecule to the surface will relocate the pre-adsorbed atomic H at the surface (green atoms). (For interpretation of the references to colour in this figure legend, the reader is referred to the web version of this article.)

Table 1
Formation of methanol at different local chemistries.

Reaction	Coverage	E_a (eV)	ΔE (eV)
1. $CO_2CH_3(s) + H(s) \rightarrow CO(s) + CH_3OH$	0.50 ML H	0.94	−0.86
2. $CO_2CH_3(s) + H(s) \rightarrow CO(s) + CH_3OH$	0.75 ML H	1.47	−1.26
3. $CO_2CH_3(s) + H(s) \rightarrow CO(s) + CH_3OH$	1.00 ML H	0.66	−0.75
4. $CH_3(s) + O(g) \rightarrow CH_2OH(s)$	–	–	−4.93
5. $CH_2OH(s) + H(s) \rightarrow CH_3OH(g)$	0.25 ML H	0.59	−0.36
6. $CH_2OH(s) + H(s) \rightarrow CH_3OH(g)$	0.50 ML H	0.56	−0.49
7. $CH_2OH(s) + H(s) \rightarrow CH_3OH(g)$	0.75 ML H	0.14	−1.47
8. $CH_2OH(s) + H(s) \rightarrow CH_3OH(g)$[a]	0.50 ML H	0.42	−0.89
9. $CH_2OH(s) + H(s) \rightarrow CH_3OH(g)$[b]	0.50 ML H	0.37	−0.51
10. $CH_2OH(s) + H(s) \rightarrow CH_3OH(g)$[a]	0.56 ML H	0.25	−0.73
11. $CH_2(s) + O(g) \rightarrow COH(s) + H(s)$	–	–	−4.68
12. $CHOH(s) + H(s) \rightarrow CH_2OH(s)$	0.75 ML H	0.39	+0.12
13. $OCH_3(s) + H(s) \rightarrow CH_3OH(g)$	0.50 ML H	0.54	+0.17
14. $OCH_3(s) + H^{(fcc)}(s) \rightarrow CH_3OH(g)$	0.62 ML H	0.35	−1.03
15. $OCH_3(s) + H^{(hcp)}(s) \rightarrow CH_3OH(g)$	0.62 ML H	0.11	−1.38
16. $OCH_3(s) + H(s) \rightarrow CH_3OH(g)$[b]	0.62 ML H	0.15	−1.04
17. $OCH_3(s) + H(s) \rightarrow CH_3OH(g)$[b]	0.75 ML H	0.37	−0.60

[a] In the presence of a neighboring $CHCH_2$ fragment.
[b] In the presence of a neighboring CCH_2 fragment.

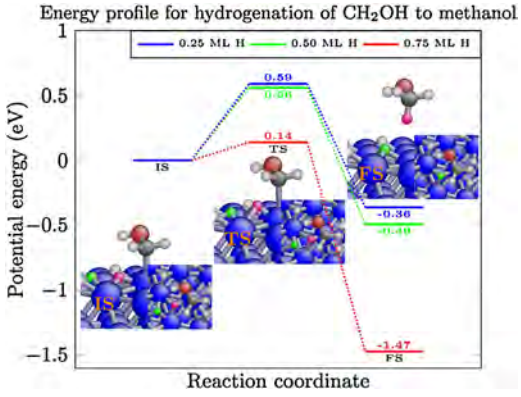

Fig. 2. Reduction in activation energy for associative desorption of methanol due to an increase of the H-coverage. Side view and top view of H-transfer (pink atom) to previously formed CH_2OH fragments are shown in the insets for a coverage of 0.75 ML of H. The associative desorption of methanol (side view) will cause the associated H diffusion at the surface (green atoms). (For interpretation of the references to colour in this figure legend, the reader is referred to the web version of this article.)

insets. This transition is considered in the associative desorption channel of methanol.

The introduction of an O atom from the plasma to an adsorbed CH_2 group is another preliminary step for the formation of methanol, as shown in Fig. S7c and d. This leads to the formation of a CHOH fragment at the surface, which is a strongly exothermic reaction by 4.68 eV (Table 1, reaction 11). An activation energy of 0.39 eV (Table 1, reaction 12) is calculated for H-transfer from a hcp site to CHOH at 0.75 ML of H-coverage, forming CH_2OH, which can then further be converted into methanol as discussed above. Fig. S8 shows a side view of this hydrogenation.

So far, the interaction of O atoms from the plasma with previously adsorbed chemical fragments derived from methane is investigated, followed by hydrogenation of the oxygenated fragments. In the following, the opposite process, i.e., the introduction of CH_3 fragments from the plasma to adsorbed O atoms will be discussed.

The introduction of a CH_3 radical to an adsorbed O atom will cause the formation of a surface-adsorbed OCH_3 fragment. The activation energy for H-transfer to this OCH_3 fragment, into the formation of methanol, at different H coverages is calculated. At low H-coverage, OCH_3 is located at a hcp site. In this circumstance, the O atom is three-coordinated. An activation energy of 0.54 eV is calculated at a coverage of 0.50 ML of H for H-transfer from a hcp site to an OCH_3 fragment (Fig. 3 and Table 1, reaction 13). This reaction is endothermic by 0.17 eV.

The introduction of more H atoms to the surface gives rise to relocation of OCH_3 to a bridging site. For instance, at 0.62 ML of H coverage, the OCH_3 fragment is transferred to a bridging site at the surface, as shown in the insets of Fig. 3. This means that the OCH_3 fragment is less tightly bound to the Ni surface and a lower activation energy for H-transfer to the fragment is expected. Indeed, an activation energy of 0.35 eV and 0.11 eV is calculated for H-transfer from a fcc and hcp site, respectively, to an OCH_3 fragment at the

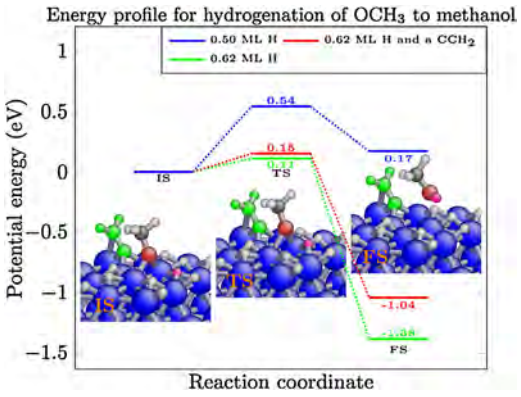

Fig. 3. Reduction in activation energy for associative desorption of methanol from an OCH_3 fragment upon higher H-coverage. An increase of the atomic H coverage facilitates the H-transfer (pink atom) from a hcp site to O of the OCH_3 fragment at the bridging site. The presence of remaining chemical fragments (green atoms) slightly increases the activation energy. The insets correspond to the red line. (For interpretation of the references to colour in this figure legend, the reader is referred to the web version of this article.)

bridging site. Both reactions are exothermic by 1.03 eV and 1.38 eV, respectively (Table 1, reaction 14 and 15). A similar relocation of H atoms at the surface, due to H-transfer to the OCH_3 fragment, is observed, as illustrated in Fig. 3. This relocation has been taken into account in the transfer channel.

To investigate the effect of remaining chemical fragments on the associative desorption of methanol from OCH_3, the activation energy of H-transfer is calculated for different local chemistries. There is no shared Ni atom between two chemical fragments. For instance, a CCH_2 fragment is considered at the Ni surface at a coverage of 0.62 ML of H (green atoms in the insets of Fig. 3). The activation energy is slightly increased from 0.11 eV to 0.15 eV for H-transfer (pink atom) to an OCH_3 fragment due to the presence of this CCH_2 fragment (Table 1, reactions 15 and 16). The H-transfer occurs from a hcp site to O of OCH_3 at the bridging site, which leads to associative desorption of methanol from the surface (see the insets in Fig. 3). An increase of the H-coverage from 0.62 to 0.75 ML gives rise to an increase in activation energy from 0.15 eV to 0.37 eV (Table 1, reaction 17). Hence, the introduction of chemical fragments at neighboring sites does not show a reduction in activation energy in this case (Table 1, reactions 16 and 17).

In plasma catalysis, fragments of oxygen compounds can be either formed in the plasma and then directly adsorb at the surface of the catalyst or formed by interaction between adsorbed and incoming fragments of CH_4 and CO_2. In both cases, facilitated associative desorption of methanol in the presence of surface-bound H atoms is observed. Hence, the low temperature production of methanol by plasma catalysis on a Ni catalyst is expected, as was indeed observed experimentally on different catalysts [12]. In this study, the experiments were carried out under atmospheric pressure and the catalyst bed was heated to a moderate temperature (<250 °C) and the plasma zone was kept at room temperature.

3.2. Hydrogenation of C_1-hydrocarbon fragments

Since the retention of fragments of methane by the metal is essential to enhance the formation of the desired products, hydrogenation of C_1-hydrocarbon fragments is discussed here. Indeed, a better retention of adsorbed hydrocarbon fragments increases the chance of forming value-added chemicals either through the ER or LH mechanism. The adsorbed chemical fragments derived from methane can be the product of dissociative adsorption of methane at the surface or they can directly be adsorbed as free radicals from the plasma. As shown above, the adsorption of plasma-created species at the surface is invariably exothermic. This means that the possibility of interaction between C_1-hydrocarbons or between a C_1-hydrocarbon and an O atom will be enhanced.

Initially, a C atom is considered at a hcp site at a coverage of 0.37 ML of H (Fig. S9). H-transfer from an fcc site to the C atom is exothermic by 0.55 eV, showing an activation barrier of 0.52 eV (Table 2, reaction 1). The surface H atoms at a higher coverage are found to be highly mobile. This makes the calculation of the activation energy for the same H atom at different coverage difficult, since this H atom was relocated to a hcp site. An activation energy of 0.25 eV and 0.34 eV is calculated for H diffusion to the bare C at 0.62 and 0.75 ML of H, respectively (Table 2, reactions 2 and 3). Since the transfer channel is defined to pass over the Ni atom, a larger activation energy is obtained. However, one should keep in mind that the concentration of C atoms in the plasma is very low and adsorbed bare C atoms at the Ni surface can readily become hydrogenated.

Next, hydrogenation of CH to CH_2 is investigated. A top view of hydrogenation of CH to CH_2 is shown in Fig. S10. An activation energy of 0.13 eV is calculated for H atoms at the fcc site to a CH fragment at the hcp site at a coverage of 0.37 ML of H. This reaction becomes barrier-less at a higher coverage of 0.5 ML of H (Table 2, reactions 4 and 5).

In Fig. S11, hydrogenation of a CH_2 fragment at a hcp site to CH_3 is illustrated. The activation energy for H-transfer (pink atom) from a fcc site is reduced from 0.63 eV at a coverage of 0.25 ML of H to 0.02 eV at a coverage of 0.5 ML of H (Table 2, reactions 6 and 7). The activation energy is also calculated in the presence of a CH_2 fragment (indicated by green atoms in Fig. S11). There is no shared Ni atom between the two fragments. In this circumstance, the activation energy is increased to 0.07 eV (Table 2, reaction 8). Hydrogenation of the chemical fragment will give rise to relocation of the CH_2 group from the hcp site to the CH_3 group at the bridging site. At higher H coverage, this relocation occurs from a hcp to a top site.

So far, the calculated activation energy for hydrogenation of CH_x (x = 0, 1, 2) fragments was low. Hence, the rate of these hydrogenation reactions is expected to be high. This implies that these reactions occur readily at relatively low H coverage and typical plasma catalysis temperatures. Hydrogenation of CH_2 to a CH_3 fragment detaches the CH_3 group from three Ni atoms at the hcp site and transfers it to a bridging or top site. Hence, in this situation, the H atoms should travel a larger distance to give rise to the associative desorption of methane. This results in a higher activation energy for hydrogenation of CH_3 followed by associative desorption of methane than for hydrogenation of CH_x (x = 0, 1, 2) fragments.

H-transfer from a hcp site to a CH_3 group at a top site is calculated for different H-coverages and in the presence of a neighboring CH_3 fragment, as depicted in Fig. 4. An activation energy of 0.66 eV is calculated for this transfer at a coverage of 0.50 ML of H (Table 2, reaction 9). To investigate the effect of remaining chemical fragments on the associative desorption of methane, another CH_3 fragment is introduced at a bridging site (green atoms in the insets of Fig. 4) and the same calculation is repeated. There is no shared Ni atom between the chemical fragments. The activation energy of associative desorption of methane is now reduced to 0.59 eV (Table 2, reaction 10). Moreover, the reaction also becomes more exothermic, i.e., from 0.21 to 0.62 eV.

The effect of increasing the atomic H coverage on the associative desorption of methane is also clear from Fig. 4. By increasing the atomic H coverage from 0.50 to 0.62 ML of H, the activation energy of the reaction is reduced from 0.66 eV to 0.35 eV and the reaction becomes more exothermic, i.e., from 0.21 eV to 0.89 eV (Table 2, reaction 11). The introduction of more H atoms will give rise to a further reduction in activation energy (i.e., to 0.18 eV at a coverage of 0.75 ML of H) and the reaction becomes even more exothermic

Table 2
Hydrogenation of C_1-hydrocarbon fragments at different local chemistries.

Reaction	Coverage	E_a (eV)	ΔE (eV)
1. C(s) + H(s) → CH(s)	0.37 ML H	0.52	−0.55
2. C(s) + H(s) → CH(s)	0.62 ML H	0.25	−0.92
3. C(s) + H(s) → CH(s)	0.75 ML H	0.34	−0.96
4. CH(s) + H(s) → CH_2(s)	0.37 ML H	0.13	−0.03
5. CH(s) + H(s) → CH_2(s)	0.50 ML H	0.00	−0.29
6. CH_2(s) + H(s) → CH_3(s)	0.25 ML H	0.63	+0.15
7. CH_2(s) + H(s) → CH_3(s)	0.50 ML H	0.02	−0.42
8. CH_2(s) + H(s) → CH_3(s)[a]	0.50 ML H	0.07	−0.43
9. CH_3(s) + H(s) → CH_4(g)	0.50 ML H	0.66	−0.21
10. CH_3(s) + H(s) → CH_4(g)[b]	0.50 ML H	0.59	−0.62
11. CH_3(s) + H(s) → CH_4(g)	0.62 ML H	0.35	−0.89
12. CH_3(s) + H(s) → CH_4(g)	0.75 ML H	0.18	−1.93

[a] In the presence of a neighboring CH_2 fragment.
[b] In the presence of a neighboring CH_3 fragment.

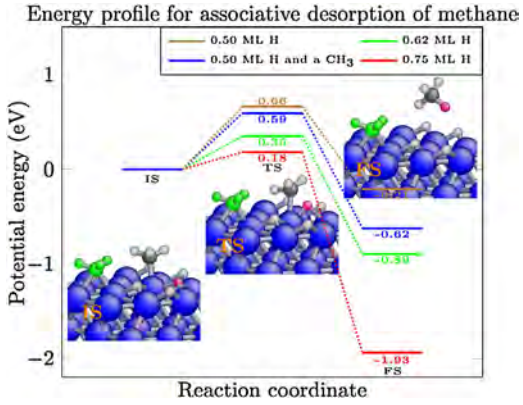

Fig. 4. Associative desorption of methane through the hydrogenation of CH_3 fragments. The presence of remaining chemical fragments (CH_3; green atoms) and the increase of the atomic H coverage facilitate the H-transfer (pink atom) from a hcp site to a CH_3 fragment at the top site. This can be seen through the reduction of the activation energy. Furthermore, the reaction also becomes more exothermic. The insets correspond to the blue line. (For interpretation of the references to colour in this figure legend, the reader is referred to the web version of this article.)

(i.e., by 1.93 eV) (Table 2, reaction 12). At a coverage of 0.62 ML of H, the Ni atom is elevated by 0.54 Å. This means that the Ni atom is situated at a higher position on the surface (green atom in Fig. S12). This value increases further to 0.56 Å at a higher coverage of 0.75 ML of H.

So far, the hydrogenation of C_1-hydrocarbon fragments was following the LH mechanism. H atoms from the plasma can also interact directly with an adsorbed C_1-hydrocarbon, which gives rise to the hydrogenation of chemical fragments or the associative desorption of methane. Moreover, this process can also happen in the opposite way, by introducing chemical fragments of methane (i.e., CH_x radicals from the plasma) to H atoms at the surface. Both reactions are exothermic. However, since both reactions follow the ER mechanism and cannot be selectively controlled by catalysis, they are not reported here.

3.3. Hydrogenation of C_2-hydrocarbon fragments

The formation of C_2-hydrocarbons can proceed either through the ER or LH mechanism. The introduction of CH_x (x = 0–3) as free radicals to an adsorbed CH_x (x = 0–3) fragment may give rise to either the formation of a closed shell molecule or the formation of an adsorbed chemical fragment.

In the former case, this may cause desorption of the formed molecule (ER mechanism). For instance, the introduction of a CH_3 fragment from the plasma to an adsorbed CH_3 group gives rise to associative desorption of ethane from the surface, since ethane adsorbs only weakly on the Ni surface. Hence, a proper flux of CH_3 fragments from the plasma and the retention of CH_3 fragments at the surface by the catalyst are key to the formation of ethane through this reaction pathway.

In the latter case, the formed chemical fragment at the surface remains adsorbed, since the open shell molecule is tightly bound to the surface. For instance, the introduction of CH_3 radicals from the plasma to an adsorbed CH_2 fragment gives rise to the formation of a CH_2CH_3 fragment. The C_2-hydrocarbon fragments may also be formed in the plasma and then become adsorbed as free radicals to the surface. When the adsorbed fragments at the surface recombine with a H atom at the surface, this gives rise to associative desorption of a formed (closed shell) molecule. This process thus follows the LH mechanism, which can be selectively controlled by choosing a proper catalyst. Hydrogenation of C_2-hydrocarbon fragments is the main subject of this section, as it can be selectively controlled by the catalyst.

Since the hydrogenation of adsorbed C and CH readily occurs at low atomic H coverage and the concentration of C and CH radicals in the plasma is low, the formation of adsorbed C_2, C_2H_2, CCH, CCH_2 and CCH_3 fragments at the surface is less likely to occur. Hence, hydrogenation of these species will not be reported here. However, it is worth to mention that the hydrogenation of these species will again be facilitated upon increasing atomic H coverage and the presence of other chemical fragments, similar to what is reported before.

First, an adsorbed $CHCH_3$ group is considered at the surface. This chemical fragment can be formed as reaction product or it can be directly adsorbed from the plasma to the surface. As shown in Fig. 5, $CHCH_3$ is located at a bridging site. The activation energy for hydrogenation of $CHCH_3$ to CH_2CH_3 is depicted in Fig. 5 for different H-coverage. The activation energy for H-transfer (pink atom) from a hcp site to $CHCH_3$ is reduced from 0.32 eV at 0.62 ML of H to 0.06 eV at 0.87 ML of H (see also Table 3, reactions 1–3). Along with the reduction in activation barrier, this reaction also becomes more exothermic, i.e., from 0.05 eV to 1.08 eV.

The activation energy is also calculated for H-transfer from a fcc site to the $CHCH_3$ group at the bridging site (Table 3, reactions 4–6). The activation energy is calculated to be 0.43 eV at a coverage of 0.75 ML of H in the absence of any other surface species (reaction 4 in Table 3). When two additional fragments of C_2-hydrocarbons (i.e., CCH_2 and $CHCH_2$) are located at the hcp site (green atoms in Fig. S13), the activation energy is increased to 0.50 eV (reaction 5 in Table 3). An increase of atomic H coverage from 0.75 to 0.81 ML of H in the presence of the same chemical fragments gives rise to a reduction in activation energy to 0.41 eV (reaction 6 in Table 3).

The next step, i.e., transfer of another H atom to the CH_2CH_3 fragment, leading to the associative desorption of ethane, is depicted in Fig. 6, for different atomic H coverages. The activation energy

Table 3
Hydrogenation of C_2-hydrocarbon fragments at different local chemistries.

Reaction	Coverage	E_a (eV)	ΔE (eV)
1. $CHCH_3(s) + H^{(hcp)}(s) \rightarrow CH_2CH_3(s)$	0.62 ML H	0.32	−0.05
2. $CHCH_3(s) + H^{(hcp)}(s) \rightarrow CH_2CH_3(s)$	0.75 ML H	0.32	−0.33
3. $CHCH_3(s) + H^{(hcp)}(s) \rightarrow CH_2CH_3(s)$	0.87 ML H	0.06	−1.08
4. $CHCH_3(s) + H^{(fcc)}(s) \rightarrow CH_2CH_3(s)$	0.75 ML H	0.43	+0.16
5. $CHCH_3(s) + H^{(fcc)}(s) \rightarrow CH_2CH_3(s)$[a]	0.75 ML H	0.50	+0.02
6. $CHCH_3(s) + H^{(fcc)}(s) \rightarrow CH_2CH_3(s)$[a]	0.81 ML H	0.41	+0.13
7. $CH_2CH_3(s) + H(s) \rightarrow CH_3CH_3(g)$	0.37 ML H	0.65	−0.28
8. $CH_2CH_3(s) + H(s) \rightarrow CH_3CH_3(g)$	0.62 ML H	0.24	−0.52
9. $CH_2CH_3(s) + H(s) \rightarrow CH_3CH_3(g)$	0.75 ML H	0.00	−1.46
10. $CHCH_2(s) + H(s) \rightarrow CH_2CH_2(s)$[b]	0.37 ML H	0.45	−0.16
11. $CH_2CH_2(s) \rightarrow CH_2CH_2(g)$	–	0.68	+0.67
12. $CH_2CH_2(s) \rightarrow CH_2CH_2(g)$[b]	0.31 ML H	0.32	+0.05
13. $CH_2CH_2(s) + H(s) \rightarrow CH_2CH_3(s)$	0.25 ML H	0.29	+0.24
14. $CH_2CH_2(s) + H(s) \rightarrow CH_2CH_3(s)$[c]	0.37 ML H	0.40	+0.18
15. $CH_2CH_2(s) + H(s) \rightarrow CH_2CH_3(s)$	0.37 ML H	0.33	+0.25
16. $CH_2CH_2(s) + H(s) \rightarrow CH_2CH_3(s)$	0.62 ML H	0.34	+0.19

[a] In the presence of CCH_2 and $CHCH_2$ fragments at the surface.
[b] In the presence of CCH_2 and CCH_3 fragments at the surface.
[c] In the presence of CCH_2 and CCH_2CH_3 fragments at the surface.

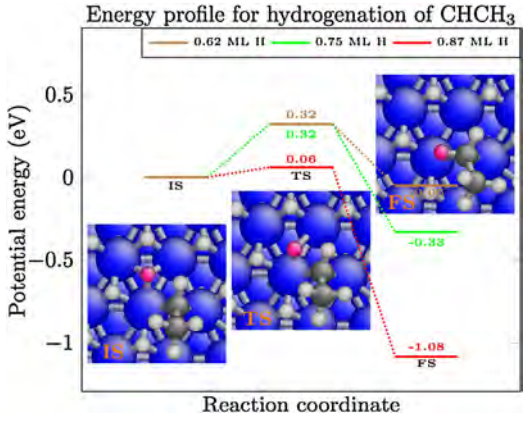

Fig. 5. Reduction in the activation energy for hydrogenation of $CHCH_3$. An increasing atomic H coverage facilitates the hydrogenation of $CHCH_3$. The H atom is transferred from a hcp site to the $CHCH_3$ group at a bridging site (insets). The insets correspond to the red line. (For interpretation of the references to colour in this figure legend, the reader is referred to the web version of this article.)

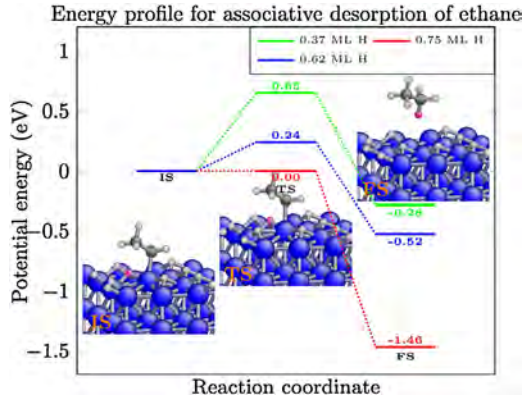

Fig. 6. Associative desorption of ethane, by recombination of a H atom from a hcp site (pink atom) and a CH_2CH_3 group at the top site. The increase in atomic H coverage reduces the activation energy and makes the reaction more exothermic. The insets correspond to the red line. (For interpretation of the references to colour in this figure legend, the reader is referred to the web version of this article.)

of H-transfer from a hcp site is reduced from 0.65 eV at a coverage of 0.37 ML of H to 0.00 eV at a coverage of 0.75 ML of H (Table 3, reactions 7–9). Thus, a higher atomic H coverage will facilitate the associative desorption of ethane. Furthermore, the reaction becomes more exothermic, from 0.28 eV to 1.46 eV.

To firmly establish a link between the reduction in activation energy and the presence of surface-bound H atoms or remaining chemical fragments at the surface, AIMD simulations are performed. Due to this reduction in activation energy, the associative desorption of ethane is no longer a rare event and the reaction should occur in a relatively short simulation time.

Three different initial configurations are considered. All configurations are initially optimized to the minimum energy (see SI: Movies 1–3). The first configuration is a CH_2CH_3 group at a top site for a coverage of 0.75 ML of H. In the second configuration, two chemical groups (CCH_2 and $CHCH_2$) are added to the first configuration. For the third one, the atomic H-coverage of the second configuration is increased to 0.87 ML of H. AIMD simulations are performed for 0.25 ps for all three configurations. Only in the third configuration, associative desorption of ethane is observed. This trend is consistent with the general reduction in activation energy due to the higher H-coverage and the presence of chemical fragments at the surface. Hence, the available thermal energy is sufficient to cross the lower activation energy and associative desorption of ethane occurs in the short period of simulation time accessible in the AIMD. Ethane production over a Ni catalyst is indeed observed in plasma catalysis at low temperature [50].

We have also studied the hydrogenation of $CHCH_2$ to CH_2CH_2. The activation energy of H transfer from a hcp site to $CHCH_2$ is calculated to be 0.45 eV, at a coverage of 0.37 ML of H and the presence of two C_2-hydrocarbon fragments (CCH_2 and CCH_3), located at hcp sites (see Fig. S14 and Table 3, reaction 10). Due to hydrogenation of the chemical fragment, it relocates from the fcc to the bridging site. In contrast to the associative desorption of ethane, hydrogenation of $CHCH_2$ will not directly lead to desorption of ethylene, since it strongly adsorbs on the bare Ni(111) surface.

Desorption of ethylene from the bare Ni(111) surface is shown in Fig. S15. A relatively large activation energy of 0.68 eV is calculated (Table 3, reaction 11). However, the presence of chemical fragments and a higher atomic H coverage at the surface will facilitate the desorption of ethylene. This is illustrated in Fig. S16, for a H-coverage of 0.31 ML of H and the presence of a CCH_2 and a CCH_3 fragment, yielding a reduction in activation energy to 0.32 eV (see reaction 12 in Table 3).

Since the activation energy for ethylene desorption is relatively high, hydrogenation of CH_2CH_2 at different atomic H coverages is also studied (Fig. S17). The activation energy for H-transfer from a hcp site to ethylene is calculated for atomic H coverages of

0.25–0.62 ML of H (Table 3, reactions 13–16). An increase of atomic H coverage from 0.25 to 0.37 ML results in a slight increase in the activation energy (reaction 15 in Table 3), and a further increases of atomic H coverage to 0.62 ML (reaction 16) does not affect the activation energy, while the presence of other chemical fragments (reaction 14) resulted in even a higher activation energy, in contrast to what was calculated so far. Since ethylene is loosely adsorbed to the surface at high atomic H coverage, H-transfer to the adsorbate is hindered. This is in good agreement with experiments where the ethylene interaction with surface-bound H atoms did not result in hydrogenation [51].

4. Conclusions

In this paper, we employed atomistic simulation at the DFT level to investigate the formation of value-added chemicals in plasma catalysis from CO_2 and CH_4 over a crystalline Ni(111) surface. We include the early stage of adsorption of free radicals of each species up to the formation of value-added chemicals. The resulting reactions, which explain the fundamental chemistry of plasma catalysis at low temperature (below 500 K), are summarized below.

4.1. Formation and desorption of methanol

The dissociation of adsorbed molecules at the surface (e.g. CO_2CH_3) to methanol and a CO molecule is facilitated by the increase of surface-bound H atoms at the crystalline Ni(111) surface. The rate of formation of methanol through this reaction pathway is likely to be accelerated by a proper choice of the catalyst. Hydrogenation of CH_3O and CH_2OH fragments leads to the formation of methanol, which is readily desorbed from the Ni(111) surface. This hydrogenation occurs by transfer of a H atom from the surface to the fragment, which can be selectively controlled by the catalyst, through the LH mechanism. The activation energy for the required H-transfer is reduced by an increase in H-coverage and other pre-adsorbed chemical fragments, and is energetically accessible at low temperature, so it should be feasible in plasma catalysis. Associated diffusion of H atoms is also observed during the course of these reactions.

4.2. Hydrogenation of C_1-hydrocarbon fragments

The retention of CH_x fragments (x = 0–3) will enhance the probability of formation of C_2-hydrocarbons and alcohols through both the LH and ER mechanisms. Hydrogenation of adsorbed CH_x (x = 0–2) fragments readily occurs at the surface. The hydrogenation of the CH_2 fragment at the surface detaches the CH_3 fragment from the three Ni atoms, and transfers it from a hcp or fcc site to a bridging or top site, depending on the H-coverage. The next hydrogenation, i.e., of CH_3, shows a larger activation energy, since the H atom must move a larger distance to lead to the associative desorption of methane. This hydrogenation is again facilitated by increasing H-coverage and the presence of neighboring chemical fragments. Hence, the aptness of a catalyst for the production of value-added chemicals in plasma catalysis can be defined as a catalyst that extends the retention of CH_x fragments in the presence of surface-bound H atoms.

4.3. Hydrogenation of C_2-hydrocarbon fragments

A higher H-coverage and the presence of chemical fragments reduce the activation energy for hydrogenation of ethane fragments and the associative desorption of ethane, so that this activation energy becomes thermally accessible at low temperature, typical for plasma catalysis. AIMD simulations firmly establish a link between the reduction in activation barrier and the probability of actually crossing this barrier. In contrast to the other hydrogenation reactions, where a reduction in activation energy was calculated upon increasing H-coverage, the opposite was shown for hydrogenation of ethylene. Hence, the surface-bound H atoms assist in desorption of a closed shell molecule from the crystalline surface rather than hydrogenation of a closed shell molecule.

In summary, we conclude that the reaction kinetics and reaction energetics of the catalytic reactions depend on the presence of surface-bound H atoms, which facilitate the catalytic reactions, and more specifically the catalytic conversion into methanol and ethane. In this circumstance, the adsorbed fragments are more loosely bound to the surface and they more easily undergo a bimolecular reaction. The same effect is also predicted in some cases when other chemical fragments are present at the surface, but sometimes also the opposite effect is observed. Finally, similar trends are observed for the formation of formaldehyde and formic acid (not presented). A summarizing, schematic diagram for the hydrogenation of an adsorbed fragment is provided in Scheme 1.

Finally, we can conclude that a wide variety of reactions can simultaneously take place at the surface during plasma catalysis. There will be a competition between the catalytic reactions at different operating temperatures and for different concentrations of plasma species, and thus fluxes to the surface, which is translated into a different elemental coverage at the surface. Their influence on the electronic structure and conformality of the catalyst surface, as well as on the eventual occurrence of the various processes, are interesting issues that we are currently investigating by incorporating the currently obtained DFT data into kinetic Monte Carlo modeling.

Acknowledgment

Financial support from the Reactive Atmospheric Plasma processing –eDucation network (RAPID), through the EU 7th Framework Programme (grant agreement no. 606889) is gratefully acknowledged. The calculations were performed using the Turing HPC infrastructure at the CalcUA core facility of the Universiteit Antwerpen, a division of the Flemish Supercomputer Center VSC, funded by the Hercules Foundation, the Flemish Government department (EWI) and the Universiteit Antwerpen.

Appendix A. Supplementary data

Supplementary data associated with this article can be found, in the online version, at http://dx.doi.org/10.1016/j.apcatb.2017.01.004.

References

[1] T.R. Karl, K.E. Trenberth, Modern global climate change, Science 302 (2003) 1719–1723.
[2] D. Pakhare, J. Spivey, A review of dry (CO2) reforming of methane over noble metal catalysts, Chem. Soc. Rev. 43 (2014) 7813–7837.
[3] V. Ponec, Some aspects of the mechanism of methanation and Fischer-Tropsch synthesis, Catal. Rev. 18 (1978) 151–171.
[4] J. Guo, H. Lou, H. Zhao, D. Chai, X. Zheng, Dry reforming of methane over nickel catalysts supported on magnesium aluminate spinels, Appl. Catal. A: Gen. 273 (2004) 75–82.
[5] X. Tu, J.C. Whitehead, Plasma dry reforming of methane in an atmospheric pressure AC gliding arc discharge: co-generation of syngas and carbon nanomaterials, Int. J. Hydrogen Energy 39 (2014) 9658–9669.
[6] S. Kameshima, K. Tamura, Y. Ishibashi, T. Nozaki, Pulsed dry methane reforming in plasma-enhanced catalytic reaction, Catal. Today 256 (Part 1) (2015) 67–75.
[7] H.L. Chen, H.M. Lee, S.H. Chen, M.B. Chang, S.J. Yu, S.N. Li, Removal of volatile organic compounds by single-stage and two-stage plasma catalysis systems: a review of the performance enhancement mechanisms, current status, and suitable applications, Environ. Sci. Technol. 43 (2009) 2216–2227.
[8] X. Tu, J.C. Whitehead, Plasma-catalytic dry reforming of methane in an atmospheric dielectric barrier discharge: understanding the synergistic effect at low temperature, Appl. Catal. B: Environ. 125 (2012) 439–448.

[9] R. Snoeckx, R. Aerts, X. Tu, A. Bogaerts, Plasma-based dry reforming: a computational study ranging from the nanoseconds to seconds time scale, J. Phys. Chem. C 117 (2013) 4957–4970.
[10] R. Snoeckx, Y.X. Zeng, X. Tu, A. Bogaerts, Plasma-based dry reforming: improving the conversion and energy efficiency in a dielectric barrier discharge, RSC Adv. 5 (2015) 29799–29808.
[11] E.C. Neyts, K. Ostrikov, M.K. Sunkara, A. Bogaerts, Plasma catalysis: synergistic effects at the nanoscale, Chem. Rev. 115 (2015) 13408–13446.
[12] L. Chen, X. Zhang, L. Huang, L. Lei, Application of in-plasma catalysis and post-plasma catalysis for methane partial oxidation to methanol over a Fe2O3-CuO/γ-Al2O3 catalyst, J. Nat. Gas Chem. 19 (2010) 628–637.
[13] A. Aziznia, H.R. Bozorgzadeh, N. Seyed-Matin, M. Baghalha, A. Mohamadalizadeh, Comparison of dry reforming of methane in low temperature hybrid plasma-catalytic corona with thermal catalytic reactor over Ni/γ-Al2O3, J. Nat. Gas Chem. 21 (2012) 466–475.
[14] R. Aerts, X. Tu, W. Van Gaens, J.C. Whitehead, A. Bogaerts, Gas purification by nonthermal plasma: a case study of ethylene, Environ. Sci. Technol. 47 (2013) 6478–6485.
[15] M. Danhua, Z. Xinbo, H. Ya-Ling, D.Y. Joseph, T. Xin, Plasma-assisted conversion of CO2 in a dielectric barrier discharge reactor: understanding the effect of packing materials, Plasma Sources Sci. Technol. 24 (2015) 015011.
[16] E.C. Neyts, A. Bogaerts, Understanding plasma catalysis through modelling and simulation—a review, J. Phys. D: Appl. Phys. 47 (2014) 224010.
[17] W. Somers, A. Bogaerts, A.C.T. van Duin, E.C. Neyts, Plasma species interacting with nickel surfaces: toward an atomic scale understanding of plasma-catalysis, J. Phys. Chem. C 116 (2012) 20958–20965.
[18] E.C. Neyts, K. Ostrikov, Nanoscale thermodynamic aspects of plasma catalysis, Catal. Today 256 (Part 1) (2015) 23–28.
[19] E.C. Neyts, Plasma-surface interactions in plasma catalysis, Plasma Chem. Plasma Process. (2015) 1–28.
[20] H.L. Chen, H.M. Lee, S.H. Chen, Y. Chao, M.B. Chang, Review of plasma catalysis on hydrocarbon reforming for hydrogen production—interaction, integration, and prospects, Appl. Catal. B: Environ. 85 (2008) 1–9.
[21] K. Hyun-Ha, K. Jong-Ho, O. Atsushi, Microscopic observation of discharge plasma on the surface of zeolites supported metal nanoparticles, J. Phys. D: Appl. Phys. 42 (2009) 135210.
[22] S. Huygh, A. Bogaerts, A.C.T. van Duin, E.C. Neyts, Development of a ReaxFF reactive force field for intrinsic point defects in titanium dioxide, Comput. Mater. Sci. 95 (2014) 579–591.
[23] S. Huygh, E.C. Neyts, Adsorption of C and CHx radicals on anatase (001) and the influence of oxygen vacancies, J. Phys. Chem. C 119 (2015) 4908–4921.
[24] M. Shirazi, S.D. Elliott, Atomistic kinetic Monte Carlo study of atomic layer deposition derived from density functional theory, J. Comput. Chem. 35 (2014) 244–259.
[25] B. Christophe De, M. Tom, D. Jan van, P. Sabine, V. Bert, C. Steven, B. Annemie, Dielectric barrier discharges used for the conversion of greenhouse gases: modeling the plasma chemistry by fluid simulations, Plasma Sources Sci. Technol. 20 (2011) 024008.
[26] C. De Bie, B. Verheyde, T. Martens, J. van Dijk, S. Paulussen, A. Bogaerts, Fluid modeling of the conversion of methane into higher hydrocarbons in an atmospheric pressure dielectric barrier discharge, Plasma Process. Polym. 8 (2011) 1033–1058.
[27] C. De Bie, J. van Dijk, A. Bogaerts, The dominant pathways for the conversion of methane into oxygenates and syngas in an atmospheric pressure dielectric barrier discharge, J. Phys. Chem. C 119 (2015) 22331–22350.
[28] M. Shirazi, S.D. Elliott, Cooperation between adsorbates accounts for the activation of atomic layer deposition reactions, Nanoscale 7 (2015) 6311–6318.
[29] M. Behrens, F. Studt, I. Kasatkin, S. Kühl, M. Hävecker, F. Abild-Pedersen, S. Zander, F. Girgsdies, P. Kurr, B.-L. Kniep, M. Tovar, R.W. Fischer, J.K. Nørskov, R. Schlögl, The active site of methanol synthesis over Cu/ZnO/Al2O3 industrial catalysts, Science 336 (2012) 893–897.
[30] F. Abild-Pedersen, J.K. Nørskov, J.R. Rostrup-Nielsen, J. Sehested, S. Helveg, Mechanisms for catalytic carbon nanofiber growth studied by \textit density functional theory calculations, Phys. Rev. B 73 (2006) 115419.
[31] N. İnoğlu, J.R. Kitchin, Simple model explaining and predicting coverage-dependent atomic adsorption energies on transition metal surfaces, Phys. Rev. B 82 (2010) 045414.
[32] T. Bligaard, J.K. Nørskov, S. Dahl, J. Matthiesen, C.H. Christensen, J. Sehested, The Brønsted–Evans–Polanyi relation and the volcano curve in heterogeneous catalysis, J. Catal. 224 (2004) 206–217.
[33] Y.-A. Zhu, D. Chen, X.-G. Zhou, W.-K. Yuan, DFT studies of dry reforming of methane on Ni catalyst, Catal. Today 148 (2009) 260–267.
[34] S.-G. Wang, X.-Y. Liao, J. Hu, D.-B. Cao, Y.-W. Li, J. Wang, H. Jiao, Kinetic aspect of CO2 reforming of CH4 on Ni(111): a density functional theory calculation, Surf. Sci. 601 (2007) 1271–1284.
[35] K.G. Prasanna, R.A. Olsen, A. Valdes, G.-J. Kroes, Towards an understanding of the vibrational mode specificity for dissociative chemisorption of CH4 on Ni(111): a 15 dimensional study, Phys. Chem. Chem. Phys. 12 (2010) 7654–7661.
[36] A. Fridman, Plasma Chemistry, Cambridge University Press, 2008.
[37] K. Tomáš, B. Annemie, Splitting of CO2 by vibrational excitation in non-equilibrium plasmas: a reaction kinetics model, Plasma Sources Sci. Technol. 23 (2014) 045004.
[38] A. Bogaerts, T. Kozak, K. van Laer, R. Snoeckx, Plasma-based conversion of CO2: current status and future challenges, Faraday Discuss. 183 (2015) 217–232.
[39] J.E. Mueller, A.C.T. van Duin, W.A. Goddard, Competing, coverage-dependent decomposition pathways for C2Hy species on nickel (111), J. Phys. Chem. C 114 (2010) 20028–20041.
[40] A. Ağıral, C. Trionfetti, L. Lefferts, K. Seshan, J.G.E. Gardeniers, Propane conversion at ambient temperatures CC and CH bond activation using cold plasma in a microreactor, Chem. Eng. Technol. 31 (2008) 1116–1123.
[41] G. Ertl, Reactions at surfaces: from atoms to complexity (nobel lecture), Angew. Chem. Int. Ed. 47 (2008) 3524–3535.
[42] G. Kresse, J. Hafner, *Ab initio* molecular dynamics for liquid metals, Phys. Rev. B 47 (1993) 558–561.
[43] P.E. Blöchl, Projector augmented-wave method, Phys. Rev. B 50 (1994) 17953–17979.
[44] J.P. Perdew, K. Burke, M. Ernzerhof, Generalized gradient approximation made simple, Phys. Rev. Lett. 77 (1996) 3865–3868.
[45] G. Kresse, J. Hafner, First-principles study of the adsorption of atomic H on Ni (111), (100) and (110), Surf. Sci. 459 (2000) 287–302.
[46] G. Kresse, J. Hafner, *Ab initio* molecular-dynamics simulation of the liquid-metal\char21{}amorphous-semiconductor transition in germanium, Phys. Rev. B 49 (1994) 14251–14269.
[47] G. Henkelman, H. Jónsson, Improved tangent estimate in the nudged elastic band method for finding minimum energy paths and saddle points, J. Chem. Phys. 113 (2000) 9978–9985.
[48] H. Jónsson, Simulation of surface processes, Proc. Natl. Acad. Sci. 108 (2011) 944–949.
[49] K.M. Bal, E.C. Neyts, Merging metadynamics into hyperdynamics: accelerated molecular simulations reaching time scales from microseconds to seconds, J. Chem. Theory Comput. 11 (2015) 4545–4554.
[50] Y. Zeng, X. Zhu, D. Mei, B. Ashford, X. Tu, Plasma-catalytic dry reforming of methane over γ-Al2O3 supported metal catalysts, Catal. Today 256 (Part 1) (2015) 80–87.
[51] S.P. Daley, A.L. Utz, T.R. Trautman, S.T. Ceyer, Ethylene hydrogenation on Ni(111) by bulk hydrogen, J. Am. Chem. Soc. 116 (1994) 6001–6002.